

This discussion paper is/has been under review for the journal *Climate of the Past* (CP).
Please refer to the corresponding final paper in CP if available.

Part 1: Experimental design and basic evaluation

M. Ballarotta et al.

A Last Glacial Maximum world-ocean simulation at eddy-permitting resolution – Part 1: Experimental design and basic evaluation

M. Ballarotta¹, L. Brodeau¹, J. Brandefelt², P. Lundberg¹, and K. Döös¹

¹Department of Meteorology/Oceanography, Stockholm University, 106 91 Stockholm, Sweden

²Department of Mechanics, KTH (Royal Institute of Technology), 106 91 Stockholm, Sweden

Received: 21 December 2012 – Accepted: 2 January 2013 – Published: 18 January 2013

Correspondence to: M. Ballarotta (maxime@misu.su.se)

Published by Copernicus Publications on behalf of the European Geosciences Union.

Title Page

Abstract

Introduction

Conclusions

References

Tables

Figures



Back

Close

Full Screen / Esc

Printer-friendly Version

Interactive Discussion



Abstract

Most state-of-the-art climate models include a coarsely resolved oceanic component, which has difficulties in capturing detailed dynamics, and therefore eddy-permitting/eddy-resolving simulations have been developed to reproduce the observed World Ocean. In this study, an eddy-permitting numerical experiment is conducted to simulate the global ocean state for a period of the Last Glacial Maximum (LGM, ~26 500 to 19 000 yr ago) and to investigate the improvements due to taking into account these higher spatial scales. The ocean general circulation model is forced by a 49-yr sample of LGM atmospheric fields constructed from a quasi-equilibrated climate-model simulation. The initial state and the bottom boundary condition conform to the Paleoclimate Modelling Intercomparison Project (PMIP) recommendations. Before evaluating the model efficiency in representing the paleo-proxy reconstruction of the surface state, the LGM experiment is in this first part of the investigation, compared with a present-day eddy-permitting hindcast simulation as well as with the available PMIP results. It is shown that the LGM eddy-permitting simulation is consistent with the quasi-equilibrated climate-model simulation, but large discrepancies are found with the PMIP model analyses, probably due to the different equilibration states. The strongest meridional gradients of the sea-surface temperature are located near 40° N and S, this due to particularly large North-Atlantic and Southern-Ocean sea-ice covers. These also modify the locations of the convection sites (where deep-water forms) and most of the LGM Conveyor Belt circulation consequently takes place in a thinner layer than today. Despite some discrepancies with other LGM simulations, a glacial state is captured and the eddy-permitting simulation undertaken here yielded a useful set of data for comparisons with paleo-proxy reconstructions.

Part 1: Experimental design and basic evaluation

M. Ballarotta et al.

Title Page

Abstract

Introduction

Conclusions

References

Tables

Figures



Back

Close

Full Screen / Esc

Printer-friendly Version

Interactive Discussion



1 Introduction

The Last Glacial Maximum (LGM) was a cold-climate event with a duration of around 6500 yr, centred approximately 23 000 yr ago (Clark et al., 2009), viz. at the end of the last glacial cycle and before the present warm phase. It is described by reconstruction techniques as the most recent maximum ice sheet extent over the continents, especially in the Northern Hemisphere with the large Laurentide and Fennoscandian ice caps over the North American and Northern European continental plateaus, respectively (Peltier, 1994, 2004; Clark and Mix, 2002). As a result of these large cryospheric changes, the sea surface was around 120 m lower than today, exposing the continental shelves to the atmosphere and hereby modifying the present-day world-ocean basins. The combination of an altered bathymetry, a changed hydrosphere and an atmosphere with lower green-house gas concentrations during this glacial phase may have led to modifications of the ocean state, e.g. the temperature and salinity distributions, the tidal mixing and dissipation (Green et al., 2009), the transports of heat, mass and sediments (Seidov and Haupt, 1997) as well as the Meridional Overturning Circulation (MOC). Consequently, this ocean state may have generated feedbacks to the global climate. The LGM hence constitutes a uniquely fascinating time slice of the Earth's climate history, which can be used for understanding climate change, for testing general circulation models under different boundary conditions, and for reconstructing past scenarios on the basis of comparisons with the paleo-record.

Reconstructions of the Earth's climate variations are based on analysing geological/biological samples (e.g. ice- and sediment cores, pollen, corals, tree-rings or speleothems) and utilising models. Paleo-proxy data were first used to define and prescribe boundary conditions for Atmospheric Global Circulation Models (AGCMs) (Gates, 1976; Toracinta et al., 2004), for AGCMs coupled with mixed-layer ocean models (Broccoli, 2000; Hewitt et al., 2003), and also for high-resolution atmospheric models (Kim et al., 2007). Subsequently it has proved possible to simulate climate variations with fully coupled ocean-atmosphere models (Braconnot et al., 2007a,b). The

Part 1: Experimental design and basic evaluation

M. Ballarotta et al.

Title Page

Abstract

Introduction

Conclusions

References

Tables

Figures



Back

Close

Full Screen / Esc

Printer-friendly Version

Interactive Discussion



Part 1: Experimental design and basic evaluation

M. Ballarotta et al.

Title Page

Abstract

Introduction

Conclusions

References

Tables

Figures



Back

Close

Full Screen / Esc

Printer-friendly Version

Interactive Discussion



Paleoclimate Modelling Intercomparison Project (PMIP) was initiated in the early 1990 s to evaluate and compare the response of numerical climate models under paleoclimate conditions. Due to computational limitations, the evaluations were undertaken using coarse-resolution models. These simulate the large-scale structures of the ocean, but usually parameterise the sub-grid-scale physics (unresolved structures), such as turbulence (see e.g. Gent and McWilliams, 1990). In eddy-permitting ocean models, the spatial resolution has been increased and the amount of sub-grid-scale parameterisation has been reduced. It has been demonstrated that for the present-day climate, eddy-permitting oceanic simulations improve the quality of the representations of the western boundary currents as well as those of the sea-ice conditions and the meridional heat transports in the North Atlantic and Southern Oceans (The FRAM Group, 1991; Treguier et al., 2005; Hallberg and Gnanadesikan, 2006; Spence, 2010). Until now, this type of simulation has only been conducted over regional scales for the LGM climate (Yang et al., 2006; Mikolajewicz, 2011).

Since these high-resolution simulations are more realistic, they will become more and more important for validating specific past oceanic scenarios (Beal et al., 2011; Condron and Winsor, 2011) and for comparisons with paleo-reconstructions (Otto-Bliesner et al., 2009). As pointed out by (Hargreaves et al., 2011), proxy-data pertain to specific locations and are valid over spatial scales which are smaller than that of the coarse-resolution model grid. The aim of the present investigation is to evaluate whether the eddy-permitting oceanic simulations improve the results with regard to coarse-resolution models and paleo-proxy reconstructions, and to understand how a global Ocean General Circulation Model (OGCM) behaves subject to glacial forcing and at the expected resolution of the next generation of global climate models. To achieve this, a glacial eddy-permitting numerical simulation, henceforth denoted LGM, has been conducted.

The experimental design is here described and the LGM model results are first discussed in relation to those from an analogous present-day (1958–2006) eddy-permitting hindcast simulation, denoted PD. This is done because most proxy-data

reconstructions of the past climate have employed calibration techniques based on the modern ocean state (Otto-Bliesner et al., 2009). The two experiments were undertaken with the same numerical model and the same parameterisations of the physics, but with different boundary conditions, cf. Table 1. A description of the model and its boundary conditions for the two configurations is provided hereafter. The LGM results are then analysed with focus on how the eddy-permitting simulation behaves compared with the available PMIP results. The prospects for the eddy-permitting simulations to be more consistent with the paleo-proxy data will be dealt with in a following paper (A Last Glacial Maximum world-ocean simulation at eddy-permitting resolution – Part 2: Confronting the paleo-proxy data).

2 Experimental design

2.1 The ocean model

The OGCM NEMO (Nucleus for European Modelling of the Ocean, Madec, 2008) is used for the two ORCA025 eddy-permitting simulations. It solves the primitive equations discretised on a Arakawa C-grid with a 0.25 degree resolution and comprises 46 depth levels with a refined mesh near the surface. A partial-step method has been used for a better representation of the bathymetry (Barnier et al., 2006). Temperature and salinity are linked to the density via a non-linear equation of state (Jackett and McDougall, 1995). The ocean model is coupled every 2 model-hours with the multi-layer thermodynamic-dynamic LIM sea-ice model version 2 (Fichefet and Maqueda, 1997). This 2-D visco-plastic model, on an Arakawa B-grid, calculates the thermodynamic growth and decay of the ice, as well as its dynamics and transport, taking into account the sub-grid-scale effects of snow and ice thickness.

Part 1: Experimental design and basic evaluation

M. Ballarotta et al.

Title Page

Abstract

Introduction

Conclusions

References

Tables

Figures



Back

Close

Full Screen / Esc

Printer-friendly Version

Interactive Discussion



2.2 The boundary conditions

For modelling the LGM climate, a reconstructed topography is required. The ICE-5G reconstruction (Peltier, 2004) includes bathymetry, altimetry and ice sheet reconstructions. The latter are based on geological insights as well as a sea-level model, whereas the geomorphology of the continental plates during the LGM is similar to those of the present day. The major difference is the emergence of the continental shelves due to a sea level approximately 120 m lower than today. In the LGM simulation, ice sheets and closed basins are considered as land points, cf. the land/sea mask in Fig. 1a.

Different techniques can be used to initialise the ocean model in the LGM simulations. The PMIP2 protocol recommends starting the integrations either by using a spin-up procedure or from a previous LGM state generated by other simulations. The former procedure is based on integrations made with pre-industrial boundary conditions, this in order to reach a cold equilibrium. Because the integration time is too long when starting from the recent-past ocean state, we have chosen the cold-state initialisation technique and an ocean at rest. The temperature and salinity fields are interpolated onto the ocean grid mesh from the quasi-equilibrated climate model integration (Brandefelt and Otto-Bliesner, 2009), and thus the LGM global-ocean averaged salinity and temperature is 36.59 PSU and 0.60 °C. In the PD simulation the ocean is fresher and warmer, 34.72 PSU and 3.60 °C (Levitus references). This salinity difference is due to the freshwater sequestered in the ice caps during the glacial era as well as the brine rejection from sea-ice formation and the model equilibrium (cf. Sect. 2.2).

The surface boundary conditions between the ocean/sea-ice and the atmosphere are determined using the NCAR bulk formulae (Large and Yeager, 2004). This is the most popular method and has been used as the reference-surface-fluxes computational method for the numerical-model evaluations in, e.g. the Drakkar experiments (Barnier et al., 2007; Brodeau, 2007).

The LGM surface atmospheric variables originate from a coupled climate simulation using the CCSM3 model. The horizontal resolution of its atmospheric component is

Part 1: Experimental design and basic evaluation

M. Ballarotta et al.

Title Page

Abstract

Introduction

Conclusions

References

Tables

Figures



Back

Close

Full Screen / Esc

Printer-friendly Version

Interactive Discussion



128 longitudinal by 64 latitudinal points (T42). The horizontal resolution of the ocean component is approximately 1° . Table 1 shows the forcing variables used for the ocean model and their corresponding periodicity. The forcing is based on a 49-yr dataset from the quasi-equilibrium LGM2 period 1412–1460 (Brandefelt and Otto-Bliesner, 2009) and thus represents a period differing from most of those used in the PMIP2 analyses. The model is integrated for 150 yr by repeating three times the atmospheric forcing and no restoring term in temperature and salinity is applied at the sea-surface since the main goal of our experiment is to investigate the impact of the ocean grid resolution on the representation of the surface state. Consequently, the salinity/temperature feedbacks on the atmosphere are not modelled.

The PD ocean configuration is forced for 49 yr with the atmospheric Drakkar Forcing Set v4.3 (DFS4.3, Brodeau et al., 2010) for the period 1958–2006 with corrections for the surface temperature and humidity, winds, incoming radiation and precipitation. Brodeau et al. (2010) showed that numerical results (e.g. the wind-driven circulation in the subtropical gyres and the ACC, the Arctic ice cover and the vertical representation of the temperature) were improved using this dataset. As in the LGM case, the frequency of the atmospheric variables follows the recommendation from Large et al. (1997). In the PD simulation, the turbulent atmospheric variables have a 6-hourly frequency, whereas the freshwater and radiative fluxes are based on monthly data. The runoff forcing is from the Global Runoff Data Centre reconstruction and also makes use of the climatology of smaller rivers (Brodeau, 2007). Table 1 sums up the forcing variables and frequencies used for the PD simulation. In this PD simulation, surface restoring terms are applied in order that the model surface state matches with the observed state.

The zonally prescribed total precipitation over the ocean for the LGM and PD experiments are shown in Fig. 10a. The PD precipitation profile has a maximum at 7° N, corresponding to the Inter-Tropical Convergence Zone (ITCZ). Secondary maxima are located in the mid-latitudes and are associated with the polar fronts. The LGM precipitation profile is almost symmetric with respect of the equator and shows maxima at

Part 1: Experimental design and basic evaluation

M. Ballarotta et al.

Title Page

Abstract

Introduction

Conclusions

References

Tables

Figures



Back

Close

Full Screen / Esc

Printer-friendly Version

Interactive Discussion



Part 1: Experimental design and basic evaluation

M. Ballarotta et al.

Title Page

Abstract

Introduction

Conclusions

References

Tables

Figures



Back

Close

Full Screen / Esc

Printer-friendly Version

Interactive Discussion



7° N and 7° S in the inter-tropical region. These stronger “double” ITCZs are observed in most climate-model simulations (Lin, 2007) and may be related to an enhanced and broader Hadley circulation in the LGM simulation. For the other latitudes, the LGM total precipitation is about $1 \times 10^{-5} \text{ kg m}^3 \text{ s}^{-1}$ ($\approx 0.86 \text{ mm day}^{-1}$) smaller than in the PD case and is thus consonant with the drier climate conditions (-1 to -4 mm day^{-1}) observed in PMIP2 model results (Braconnot et al., 2007a). The PD snow precipitation over the ocean, cf. Fig. 10b, takes place in the polar regions (above 40° latitude). In the LGM experiment, the profile and maxima are shifted between 10 and 20 degrees equatorwards in both hemispheres. The polar regions receive less snow due to drier condition caused by the sea-ice and the ice-caps, but the snow cover in the mid-latitudes is 10–30 % higher (Braconnot et al., 2007b).

The zonally-averaged specific humidity profiles in Fig. 10c show that the LGM surface is around 1 g kg^{-1} drier between the poles and the tropics compared to the PD conditions. In the inter-tropical band, the LGM surface is around $2\text{--}3 \text{ g kg}^{-1}$ drier due to the reduced precipitation. Therefore, associated with the reduced greenhouse-gas concentration, the LGM 2-m temperature in this region is around 3°C colder than in the PD results (Fig. 10d), which is consistent with most PMIP2 simulations (Braconnot et al., 2007a). As a consequence of the cold and dry surface conditions, the difference between these datasets reaches almost 20°C near the poles and the effects of the LGM shortwave solar radiation become stronger in the polar and inter-tropical regions (Fig. 10e). The long-wave radiation (Fig. 10f) is similarly smaller in the LGM case since this is characterised by a lower cloud cover and lower greenhouse-gas concentrations.

The latitudinally averaged zonal and meridional winds are shown in Fig. 10g and h. Due to the changes of the meridional temperature gradient, the mid-latitude winds are stronger and shifted equatorwards during the glacial period compared with PD conditions (Toggweiler et al., 2006). In the inter-tropical band, the winds are rather similar near the equator, but are around 1 m s^{-1} stronger in the Tropics during the LGM. In the polar regions, the LGM winds are stronger, most likely due to enhanced katabatic winds from the Antarctic and North American ice sheets.

3 Effect of the glacial forcing

In this section, the LGM “eddy-permitting” results are analysed and compared with those from the analogous PD eddy-permitting simulation and the PMIP-model results. The diagnostics conform to those used in the Ocean-Sea-ice model intercomparison experiment (Griffies et al., 2009).

3.1 The ocean surface

The simulated LGM time-averaged Sea Surface Temperature (SST) distribution was found to be almost symmetric around the equator with the strongest meridional gradients in the mid-latitude regions (Fig. 1a). The North Atlantic, the North Pacific, the Arctic and the Antarctic show a tendency toward cold surface temperatures due to the sea-ice cover. The highest SSTs are found in the equatorial region of the western Pacific and the eastern Atlantic, and the eastern and equatorial Pacific cold tongue is also captured. These features are consistent with those in the PMIP2 simulations (Otto-Bliesner et al., 2009). Compared with the PD results, the global ocean SSTs are predominantly lower (Fig. 1b). Maximum deviations are found in the North Atlantic (more than 10 °C), the North Pacific (4 to 8 °C) and in the northern branch of the Antarctic Circumpolar Current, ACC, (4 to 7 °C), all due to the presence of sea-ice. In the polar regions covered by sea-ice, the deviations from the PD SSTs are reduced. As noted for the PMIP2 models, the cooling may be as large as -3 °C in the Indian and Pacific Oceans, but is about 1 °C less in the tropical Atlantic. However, two areas near the coasts of Chile and Namibia show positive anomalies. Under present-day conditions, cold upwelling takes place in these regions. This warm SST bias is generally associated with a poor representation of the upwelling processes in the numerical models.

The simulated LGM time-averaged Sea Surface Salinity (SSS), cf. Fig. 2a, shows that the most saline surface waters are found in the Southern Ocean (brought about by brine rejection), the South Tropical band and with maxima in the Tropical Atlantic and Mediterranean (due to evaporation). Two surface waters face each other in the

Part 1: Experimental design and basic evaluation

M. Ballarotta et al.

Title Page

Abstract

Introduction

Conclusions

References

Tables

Figures

⏪

⏩

◀

▶

Back

Close

Full Screen / Esc

Printer-friendly Version

Interactive Discussion



North Atlantic: the warm, saline tropical water and the cold, fresh mid-latitude water created by sea-ice melting. Fresher surface waters are found at river mouths (e.g. the Congo and Mackenzie Rivers) and over the littoral where the ice-sheets melt. As a consequence of the fresh water stored in the continental ice-caps, the LGM SSS is globally higher than the PD SSS (Fig. 2b). The largest differences compared with the PD experiment are found in the polar regions, where the sea-ice formation at the ocean surface rejects brine, which participates in the densification of the waters (Otto-Bliesner et al., 2007). In the Arctic region, the SSS is also higher due to the reduced river runoffs in the LGM experiment. In the South equatorial Pacific and Atlantic, LGM-simulated SSSs are fresher due to more precipitation during the glacial period (cf. Fig. 10a). However, the LGM eddy-permitting SSSs appear to be around 1 PSU higher than in the coupled ocean-atmosphere experiments reported by (Shin et al., 2003). This difference can be inferred from the initial-state salinity rise applied in the CCSM simulation, and is consequently recovered in our LGM simulation since it started from a CCSM3 equilibrated state.

The mixed-layer-depth (MLD) patterns of the two simulations shows discrepancies (Fig. 3a, b). The mixed layer is calculated as the maximum depth h where the potential density difference $\Delta\rho$ between the surface and h is smaller than 0.01 kg m^{-3} . This diagnostic is an indicator for the thermocline ventilation and the deep-water formation. For the PD period, the maximum MLDs are found in the North Atlantic (at the entrance to the Labrador, Greenland and Norwegian Seas) and are associated with the formation of North Atlantic Deep Water (NADW). In the Southern Hemisphere, the deep mixed-layers are located in the South-East-Pacific ACC region where Subantarctic Mode Water (SAMW) and Antarctic Bottom Water (AABW) are formed. In the LGM simulation, the deep mixed layers are found in the region, where thick sea-ice is formed and where the warm and saline tropical waters encounter the cold and fresh conditions near the sea-ice edge. In the Northern Hemisphere, deep-water formation hence takes place in the Arctic basin and near 30° N , suggesting that the LGM Atlantic circulation may differ from that of the PD case. In the Southern Hemisphere, this process takes

Part 1: Experimental design and basic evaluation

M. Ballarotta et al.

Title Page

Abstract

Introduction

Conclusions

References

Tables

Figures

⏪

⏩

◀

▶

Back

Close

Full Screen / Esc

Printer-friendly Version

Interactive Discussion



place in the northern branch of the ACC and along the coast of Antarctica (adjacent to the Weddell and Ross Seas), also here associated with the sea-ice dynamics. These changes are also noted in the equilibrated simulation by (Brandefelt and Otto-Bliesner, 2009) with a MLD that is reduced in the North Atlantic and increased in the Weddell Sea.

The LGM sea-ice cover is larger than in the PD simulation (Fig. 4). The sea-ice area is increased by a factor 1.5 in the Northern Hemisphere and by 11.8 in the Southern Hemisphere during the boreal winter. During summer it increases by a factor 1.7 and 2.4 in the Northern and Southern Hemisphere, respectively. Although the area of the sea-ice is larger in the Southern Hemisphere, its volume is greater in the Northern Hemisphere (cf. Fig. 5) due to the formation of thicker sea-ice in the Arctic region. The LGM volume of sea-ice in the Southern Ocean is about 10 times larger than in the PD experiment, compared to a value of 5 times for the Arctic. Moreover, the seasonal variability of the Southern-Ocean sea-ice volume is around $20000 \times 10^9 \text{ m}^3$ in the LGM case and $10000 \times 10^9 \text{ m}^3$ in the PD simulation. In contrast, the LGM seasonality is slightly reduced in the Northern Hemisphere, probably due to a more zonal propagation of the Gulf stream during this period. In the Southern Ocean, the seasonal variability is larger, most likely controlled by the large formation of sea-ice during the austral winter. The LGM sea-ice cover is consistent with the CCSM3 simulation undertaken by (Brandefelt and Otto-Bliesner, 2009), which showed an increasing trend for the sea-ice fraction (especially in the Northern Hemisphere) at the second equilibrated stage. Increasing trends have been observed in almost all PMIP2 models (Braconnot et al., 2007b), but their magnitudes differed. It has also been noted that CCSM3 simulates an approximately 50% larger sea-ice area in the Southern Ocean than the other PMIP models (Murakami et al., 2008). Consequently, the seasonality of the Southern-Ocean sea-ice cover is not captured by the eddy-permitting simulation and our results are thus not fully consistent with the paleo-reconstructions. For the boreal winter, the model simulates sea-ice cover in the Nordic Seas, the northwestern North Atlantic and the Labrador Sea, and the North Atlantic sea-ice extent reaches almost 40° N . The central

Part 1: Experimental design and basic evaluation

M. Ballarotta et al.

Title Page

Abstract

Introduction

Conclusions

References

Tables

Figures



Back

Close

Full Screen / Esc

Printer-friendly Version

Interactive Discussion



Arctic basin and western Fram Strait have perennial sea-ice. In the Southern Ocean, the austral summer sea-ice edge is located near 50° S between 60° W and 120° E and near 55° S in the rest of the circumpolar region. For the boreal summer, the LGM sea-ice fraction is reduced in the Labrador Sea, the Central North Atlantic basin and the Norwegian Sea, suggesting possibly ice-free conditions during the glacial period (see the animation available as Supplement).

3.2 The zonal structure of the ocean

The impact of the glacial forcing on the vertical structure of the ocean is analysed in terms of the zonally-averaged temperature and salinity. Fig. 6a presents the former quantity in the simulated LGM global ocean. This glacial-ocean vertical structure shows that the Arctic, the Antarctic, the North Atlantic (north of 60° N) and the deep ocean (below ~ 1000 m) are relatively cold (below 1°C) compared to the inter-tropical ocean surface. In addition, the effect of the sea-ice cover in the North Atlantic region tends to decrease the temperature in the uppermost 100 m between 40° N and 60° N. In comparison with the PD simulation (Fig. 6b), the smallest anomalies (less than 1°C) are found in the regions prone to a glacial state under present-day conditions, i.e. in the Arctic surface and deep-waters as well as in the Antarctic surface water. On the other hand, the largest differences are found in the North Atlantic surface water covered by sea-ice between 30 and 70° N and in the Antarctic Intermediate Water (AAIW), where the cold and dense surface waters from the sea-ice edge plunge to feed the deep ocean. In this latter region, the LGM ocean is between 2 and 3°C colder than in the PD simulation, consistent with the deep-ocean reconstruction due to Adkins et al. (2002).

The zonally-averaged salinity during the LGM is shown in Fig. 7a. Here the deep ocean is represented as horizontal layers of fluid of different salinities, from 36 PSU at a depth of ~ 1000 m to 37.25 below ~ 3000 m. The most saline waters are found in the deep Southern Ocean, consistent with paleo-reconstructions by Adkins et al. (2002). In the upper layer (above 1000 m), five features are of particular interest:

Part 1: Experimental design and basic evaluation

M. Ballarotta et al.

Title Page

Abstract

Introduction

Conclusions

References

Tables

Figures



Back

Close

Full Screen / Esc

Printer-friendly Version

Interactive Discussion



Part 1: Experimental design and basic evaluation

M. Ballarotta et al.

Title Page

Abstract

Introduction

Conclusions

References

Tables

Figures

◀

▶

◀

▶

Back

Close

Full Screen / Esc

Printer-friendly Version

Interactive Discussion



1. The Southern-Ocean brine-rejection-induced highly saline waters plunging to feed the deep ocean.
2. The AAIW-associated fresher (34.25–35.5 PSU) waters in the northern front of the ACC due to sea-ice melting.
3. The equatorial surface water of low salinities (35–35.5 PSU) caused by precipitation.
4. The saline waters of Mediterranean origin at around 35° N.
5. The fresh surface waters of the North Atlantic, the North Pacific and the Arctic resulting from sea-ice melting.

The LGM global ocean is characterised by higher salinities than those in the PD simulation (Fig. 7b). The differences are most pronounced in the deep ocean with an additional salinity of 1.5–2.5 PSU due to brine rejection in the polar-region surface waters that are mixed vertically (Brandefelt and Otto-Bliesner, 2009). Slightly fresher surface waters are noted in the Northern Hemisphere where sea-ice melting takes place between 40 and 60° N as well as between the equator and 20° S, here due to increased precipitation. It is, however, suggested that the LGM ocean salinity increases on average by 1 PSU everywhere (PMIP2 recommendation). The 2-PSU difference between the two eddy-permitting simulations presented here is probably due to two factors: pro primo, it has already been noted that the CCSM LGM simulation shows a higher salinity content than the other models. This has been attributed to the 1-PSU salinity rise applied to this simulation (Murakami et al., 2008). Consequently, our LGM initial state starts with this bias. Pro secundo, the important formation of sea-ice in the equilibrated state and an increased AABW may contribute in the release and diffusion of brine and thus modify the salt content of the deep ocean. As pointed out in connection with other numerical simulations (Kim et al., 2002; Shin et al., 2003; Brandefelt and Otto-Bliesner, 2009), the formation of a large volume of sea-ice can have an impact on the ocean salinity content due to the brine rejection.

3.3 The transports of mass and heat

The LGM and PD Atlantic meridional overturning circulations (AMOCs) are characterised by a northward surface-water transport, a sinking of dense waters at high latitudes and a deep return flow towards the Southern Ocean (Fig. 8a, b). Due to the changes of the convection regions, the sinking takes place between 30 and 65° N in the LGM simulation, and between 40 and 80° N in the PD experiment. The return flow in the LGM simulation is found at a shallower depth (~ 1000 m) than in the PD case (~ 3500 m), mainly due to the larger intrusion of the Antarctic Bottom Water (AABW) into the world-ocean basins. Most of the thermohaline circulation is thus “squeezed” into a thinner layer. The weakening of the LGM overturning is also observed in the AMOC maximum, which is 10 Sv for the LGM simulation compared to 17 Sv for the PD experiment. This maximum is however smaller in the eddy-permitting simulation than those found from the PMIP2 models, which range from 13.8 to 20.8 Sv (Otto-Bliesner et al., 2007). On the other hand, an analogous reduction has also been observed in the equilibrated simulation by Brandefelt and Otto-Bliesner (2009), who also noted an equatorward shift of the convection sites from the Greenland-Iceland-Norwegian seas to 30° N.

As a consequence of the reduced AMOC, the northward heat transport in the Atlantic basin is on average reduced by 0.25 PW between 35° S and 35° N (Fig. 9), reaching a maximum of 0.6 PW near 25° N. The transport is close to zero in the South Atlantic basin, suggesting that the global tropical cooling is achieved by a stronger meridional heat transport in the Indo-Pacific basin. Therefore, the meridional heat transport for the LGM global ocean attains a maximum of 1.5 PW near 15° N and 15° S. Between 40 and 90° N, and between 50° S and 80° S, the LGM meridional transport of heat is smaller than in the PD experiment due to the presence of sea-ice. These features are consistent with previous model diagnostics (Ganopolski et al., 1998; Weaver et al., 1998; Hewitt et al., 2001), but not with recent PMIP2 model results, which show larger transports between 40 and 60° N for the global ocean, a larger transport in the Atlantic basin

Part 1: Experimental design and basic evaluation

M. Ballarotta et al.

Title Page

Abstract

Introduction

Conclusions

References

Tables

Figures



Back

Close

Full Screen / Esc

Printer-friendly Version

Interactive Discussion



(south of 30° N) and a smaller transport in the Pacific (south of 40° N) (Murakami et al., 2008). These large discrepancies are connected with the differences in the meridional overturning circulations and the reorganization of the temperatures (due to the sea-ice formation) between our equilibrium and those in the PMIP2 models.

4 Summary and outlook

This study presents the response of the first global eddy-permitting Ocean General Circulation Model forced with atmospheric fields representing a 49-yr sample of the Last Glacial Maximum climate. The numerical results are compared with those from a realistic reference experiment carried out with the same ocean model but representing present-day (1958–2006) conditions. This comparison shows that the simulated glacial ocean is globally colder and has a higher salinity than in the present-day experiment. A thicker sea-ice cover spreads over the mid-latitudes, reaching the latitudes of the Bay of Biscay and Cape Horn in the northern and Southern Hemisphere, respectively. The LGM meridional heat transport is larger in the Indo-Pacific basin and smaller in the Atlantic basin due to the presence of this large sea-ice cover. De facto, the meridional overturning reveals a weaker North Atlantic Deep Water circulation due to an enhanced spreading of Antarctic Bottom Water spreading through a thicker layer and the shift of the deep mixed-layers.

The results reported here are consistent with those from the source CCSM3 quasi-equilibrated simulation (Brandefelt and Otto-Bliesner, 2009), but in other respects may differ from the PMIP model analyses. As pointed out by (Brandefelt and Otto-Bliesner, 2009), their “new equilibrium differs substantially from the first quasi steady state with 1.1 °C colder global mean temperature and regional differences of 5–15 °C in the North Atlantic region and a 30 % reduction of the strength of the AMOC”. The most significant discrepancies have been diagnosed for the seasonality of the Southern Ocean sea-ice fractions. As a consequence of the larger sea-ice areas simulated in the LGM eddy-permitting model, the global ocean salinity is higher than previously reported and

Part 1: Experimental design and basic evaluation

M. Ballarotta et al.

Title Page

Abstract

Introduction

Conclusions

References

Tables

Figures



Back

Close

Full Screen / Esc

Printer-friendly Version

Interactive Discussion



the deep-water formation is modified. Nonetheless, the tropical SSTs seem to be in good agreement with previous model-based results, whereas the upwelling processes near the coast of Chile and Namibia are still poorly represented. The representation of the AMOC is also consistent with the (Brandefelt and Otto-Bliesner, 2009) simulation and is characterised by a shallower and weaker overturning compared with the PMIP2 simulations.

It appears that most of the discrepancies between the results of our simulation and those from the PMIP2 models originate from our choice of equilibrated period for the initial state. The reason why the second CCSM3 model equilibrium is chosen in the design of our eddy-permitting simulation is that this equilibrated state lasts longer than the first one in the CCSM3 climate simulation. This choice may have had a substantial impact on our eddy-permitting numerical representation of the LGM ocean state, a fact that reinforces the need to define a criterion for when a simulated climate has reached an equilibrium under the imposed forcing and PMIP boundary conditions (Brandefelt and Otto-Bliesner, 2009). The present study has nevertheless shown that it is possible to reproduce the pattern of the LGM ocean state with an eddy-permitting model and an atmospheric state constructed from a coarse-resolution climate simulation. Hence, it is now commendable to analyse the efficiency of this eddy-permitting simulation with regard to the reconstructed surface state based on paleo-proxy records. This issue is addressed in the second part of this study.

Supplementary material related to this article is available online at:
<http://www.clim-past-discuss.net/9/297/2013/cpd-9-297-2013-supplement.zip>

Acknowledgements. This work has been financially supported by the Bert Bolin Centre for Climate Research and by the Swedish Research Council. The Swedish National Infrastructure for Computing (SNIC) is gratefully acknowledged for providing the computer time on the Vagn and Ekman facilities funded by the Knut and Alice Wallenberg foundation. Many thanks to Qiong Zhang and Nathalie Pluchon for their advices and comments.

Part 1: Experimental design and basic evaluation

M. Ballarotta et al.

Title Page

Abstract

Introduction

Conclusions

References

Tables

Figures



Back

Close

Full Screen / Esc

Printer-friendly Version

Interactive Discussion



References

- Adkins, J. F., Mcintyre, K., and Schrag, D. P.: The salinity, temperature, and $\delta^{18}\text{O}$ of the glacial deep ocean, *Science*, 288, 1769–1773, doi:10.1126/science.1076252, 2002. 308
- Ballarotta, M., Döös, K., Lundberg, P., Brodeau, L., and Brandsfelt, J.: A Last Glacial Maximum World-Ocean simulation at eddy-permitting resolution – Part 2: Confronting the paleo-proxy data, *Clim. Past Discuss.*, 9, 329–350, doi:10.5194/cpd-9-329-2013, 2013.
- Barnier, B., Madec, G., Penduff, T., Molines, J.-M., Treguier, A.-M., Le Sommer, J., Beckmann, A., Biastoch, A., Böning, C., Dengg, J., Derval, C., Durand, E., Gulev, S., Remy, E., Talandier, C., Theetten, S., Maltrud, M., McClean, J., and Cuevas, B.: Impact of partial steps and momentum advection schemes in a global ocean circulation model at eddy-permitting resolution, *Ocean Dynam.*, 56, 543–567, doi:10.1007/s10236-006-0082-1, 2006. 301
- Barnier, B., Brodeau, L., Le Sommer, J., Molines, J.-M., Penduff, T., Theetten, S., Treguier, A.-M., Madec, G., Biastoch, A., Böning, C., Dengg, J., Gulev, S., Bourdalle Badie, R., Chanut, J., Garric, G., Alderson, S., Coward, A., de Cuevas, B., New, A., Haines, K., Smith, G., Drijfhout, S., Hazeleger, W., Severijns, C., and Myers, P.: Eddy-permitting ocean circulation hindcasts of past decades, *CLIVAR Exchanges Newsletter*, 42, 8–10, 2007. 302
- Beal, L. M., De Ruijter, W. P. M., Biastoch, A., Zahn, R., Cronin, M., Hermes, J., Lutjeharms, J., Quartly, G., Tozuka, T., Baker-Yeboah, S., Bormman, T., Cipollini, P., Dijkstra, H., Hall, I., Park, W., Peeters, F., Penven, P., Ridderinkhof, H., and Zinke, J.: On the role of the Agulhas system in ocean circulation and climate, *Nature*, 472, 429–436, doi:10.1038/nature09983, 2011. 300
- Braconnot, P., Otto-Bliesner, B., Harrison, S., Jousseaume, S., Peterchmitt, J.-Y., Abe-Ouchi, A., Crucifix, M., Driesschaert, E., Fichet, Th., Hewitt, C. D., Kageyama, M., Kitoh, A., Laîné, A., Loutre, M.-F., Marti, O., Merkel, U., Ramstein, G., Valdes, P., Weber, S. L., Yu, Y., and Zhao, Y.: Results of PMIP2 coupled simulations of the Mid-Holocene and Last Glacial Maximum – Part 1: experiments and large-scale features, *Clim. Past*, 3, 261–277, doi:10.5194/cp-3-261-2007, 2007a. 299, 304
- Braconnot, P., Otto-Bliesner, B., Harrison, S., Jousseaume, S., Peterchmitt, J.-Y., Abe-Ouchi, A., Crucifix, M., Driesschaert, E., Fichet, Th., Hewitt, C. D., Kageyama, M., Kitoh, A., Loutre, M.-F., Marti, O., Merkel, U., Ramstein, G., Valdes, P., Weber, L., Yu, Y., and Zhao, Y.: Results of PMIP2 coupled simulations of the Mid-Holocene and Last Glacial Maximum –

Part 1: Experimental design and basic evaluation

M. Ballarotta et al.

Title Page

Abstract

Introduction

Conclusions

References

Tables

Figures

⏪

⏩

◀

▶

Back

Close

Full Screen / Esc

Printer-friendly Version

Interactive Discussion



Part 1: Experimental design and basic evaluation

M. Ballarotta et al.

Title Page

Abstract

Introduction

Conclusions

References

Tables

Figures

◀

▶

◀

▶

Back

Close

Full Screen / Esc

Printer-friendly Version

Interactive Discussion



- Part 2: feedbacks with emphasis on the location of the ITCZ and mid- and high latitudes heat budget, *Clim. Past*, 3, 279–296, doi:10.5194/cp-3-279-2007, 2007b. 299, 304, 307
- Brandefelt, J. and Otto-Bliesner, B. L.: Equilibration and variability in a Last Glacial Maximum climate simulation with CCSM3, *Geophys. Res. Lett.*, 36, 1–5, doi:10.1029/2009GL040364, 2009. 302, 303, 307, 309, 310, 311, 312
- 5 Broccoli, A. J.: Tropical cooling at the Last Glacial Maximum: an atmosphere-mixed layer ocean model simulation, *J. Climate*, 13, 951–976, doi:10.1175/1520-0442(2000)013<0951:TCATLG>2.0.CO;2, 2000. 299
- Brodeau, L.: Contribution à l'amélioration de la fonction de forçage des modèles de circulation générale océanique, Ph. D. thesis, Université Joseph Fourier, Grenoble 1, Grenoble, France, 2007. 302, 303
- 10 Brodeau, L., Barnier, B., Treguier, A.-M., Penduff, T., and Gulev, S.: An ERA40-based atmospheric forcing for global ocean circulation models, *Ocean Model.*, 31, 88–104, doi:10.1016/j.ocemod.2009.10.005, 2010. 303
- 15 Clark, P. U. and Mix, A.: Ice sheets and sea level of the Last Glacial Maximum, *Quaternary Sci. Rev.*, 21, 1–7, doi:10.1016/S0277-3791(01)00118-4, 2002. 299
- Clark, P. U., Dyke, A. S., Shakun, J. D., Carlson, A. E., Clark, J., Wohlfarth, B., Mitrovica, J. X., Hostetler, S. W., and McCabe, A. M.: The Last Glacial Maximum, *Science*, 325, 710–714, doi:10.1126/science.1172873, 2009. 299
- 20 Condron, A. and Winsor, P.: A subtropical fate awaited freshwater discharged from glacial Lake Agassiz, *Geophys. Res. Lett.*, 38, 1–5, doi:10.1029/2010GL046011, 2011. 300
- Fichefet, T. and Maqueda, M. A. M.: Sensitivity of a global sea ice model to the treatment of ice thermodynamics and dynamics, *J. Geophys. Res.*, 102, 12609–12646, doi:10.1029/97JC00480, 1997. 301
- 25 Gates, W.: Modeling the ice-age climate, *Science*, 191, 1138–1144, 1976. 299
- Ganopolski, A., Rahmstorf, S., Petoukhov, V., and Claussen, M.: Simulation of modern and glacial climates with a coupled global model of intermediate complexity, *Nature*, 391, 351–356, doi:10.1038/34839, 1998. 310
- Gent, P. and McWilliams, J.: Isopycnal mixing in Ocean Circulation models, *J. Phys. Oceanogr.*, 20, 150–155, doi:10.1175/1520-0485(1990)020<0150:IMIOCM>2.0.CO;2, 1990. 300
- 30 Green, J. A. M., Green, C. L., Bigg, G. R., Rippeth, T. P., Scourse, J. D., and Uehara, K.: Tidal mixing and the meridional overturning circulation from the Last Glacial Maximum, *Geophys. Res. Lett.*, 36, 1–5, doi:10.1029/2009GL039309, 2009. 299

Part 1: Experimental design and basic evaluation

M. Ballarotta et al.

Title Page

Abstract

Introduction

Conclusions

References

Tables

Figures

◀

▶

◀

▶

Back

Close

Full Screen / Esc

Printer-friendly Version

Interactive Discussion



- Griffies, S. M., Biastoch, A., Böning, C., Bryan, F., Danabasoglu, G., Chassignet, E. P., England, M. H., Gerdes, R., Haak, H., Hallberg, R. W., Hazeleger, W., Jungclaus, J., Large, W. G., Madec, G., Pirani, A., Samuels, B. L., Scheinert, M., Sen Gupta, A., Severijns, C. A., Simons, H. L., Treguier, A. M., Winton, M., Yeager, S., and Yin, J.: Coordinated Ocean-Ice Reference Experiment (COREs), *Ocean Model.*, 26, 1–46, doi:10.1016/j.ocemod.2008.08.007, 2009. 305
- Hallberg, R., and Gnanadesikan, A.: The role of eddies in determining the structure and response of the wind-driven Southern Hemisphere overturning: results from the Modeling Eddies in the Southern Ocean (MESO) project, *J. Phys. Oceanogr.*, 36, 2232–2252, 2006. 300
- Hargreaves, J. C., Paul, A., Ohgaito, R., Abe-Ouchi, A., and Annan, J. D.: Are paleoclimate model ensembles consistent with the MARGO data synthesis?, *Clim. Past*, 7, 917–933, doi:10.5194/cp-7-917-2011, 2011. 300
- Hewitt, C., Broccoli, A., Mitchell, J., and Stouffer, R.: A coupled model study of the last glacial maximum: was part of the North Atlantic relatively warm?, *Geophys. Res. Lett.*, 28, 1571–1574, doi:10.1029/2000GL012575, 2001. 310
- Hewitt, C., Stouffer, R., Broccoli, A., Mitchell, J., and Valdes, P.: The effect of ocean dynamics in a coupled GCM simulation of the Last Glacial Maximum, *Clim. Dynam.*, 20, 203–218, doi:10.1007/s00382-002-0272-6, 2003. 299
- Jackett, D. and McDougall, T.: Minimal adjustment of hydrostatic profiles to achieve static stability, *J. Atmos. Ocean. Tech.*, 12, 381–389, doi:10.1175/1520-0426(1995)012<0381:MAOHPT>2.0.CO;2, 1995. 301
- Kim, S.-J., Flato, G., Boer, G., and McFarlane, N.: A coupled climate model simulation of the Last Glacial Maximum, Part 1: Transient multi-decadal response, *Clim. Dynam.*, 19, 515–537, doi:10.1007/s00382-002-0243-y, 2002. 309
- Kim, S.-J., Crowley, T. J., Erickson, D. J., Govindasamy, B., Duffy, P. B., and Lee, B. Y.: High-resolution climate simulation of the Last Glacial Maximum, *Clim. Dynam.*, 31, 1–16, doi:10.1007/s00382-007-0332-z, 2007. 299
- Large, W. G. and Yeager, S.: Diurnal to decadal global forcing for ocean and sea-ice models: the data sets and flux climatologies, NCAR technical note: NCAR/TN-460+ STR, CGD (May), National center for Atmospheric Research, Boulder, Colorado, 2004. 302
- Large, W. G., Danabasoglu, G., Doney, S. C., and McWilliams, J. C.: Sensitivity to surface forcing and boundary layer mixing in a global ocean model: annual-mean climatology, *J. Phys.*

Part 1: Experimental design and basic evaluation

M. Ballarotta et al.

Title Page

Abstract

Introduction

Conclusions

References

Tables

Figures

◀

▶

◀

▶

Back

Close

Full Screen / Esc

Printer-friendly Version

Interactive Discussion



Oceanogr., 27, 2418–2447, doi:10.1175/1520-0485(1997)027<2418:STSFAB>2.0.CO;2, 1997. 303

Lin, J.-L.: The double-ITCZ problem in IPCC AR4 coupled GCMs: ocean–atmosphere feedback analysis, *J. Climate*, 20, 4497–4525, doi:10.1175/JCLI4272.1, 2007. 304

5 Madec, G.: NEMO ocean engine, Note du Pôle de modélisation de l'Institut Pierre-Simon Laplace No 27 (27), 2008. 301

Mikolajewicz, U.: Modeling Mediterranean Ocean climate of the Last Glacial Maximum, *Clim. Past*, 7, 161–180, doi:10.5194/cp-7-161-2011, 2011. 300

10 Murakami, S., Ohgaito, R., Abe-Ouchi, A., Crucifix, M., and Otto-Bliesner, B.: Global-scale energy and freshwater balance in glacial climate: a comparison of three PMIP2 LGM simulations, *J. Climate*, 21, 5008–5033, doi:10.1175/2008JCLI2104.1, 2008. 307, 309, 311

Otto-Bliesner, B., Hewitt, C., Marchitto, T., Brady, E., Abe-Ouchi, A., Crucifix, M., Murakami, S., and Weber, S. L.: Last Glacial Maximum ocean thermohaline circulation: PMIP2 model intercomparisons and data constraints, *Geophys. Res. Lett.*, 34, 1–6, doi:10.1029/2007GL029475, 2007. 306, 310

15 Otto-Bliesner, B. L., Schneider, R., Brady, E. C., Kucera, M., Abe-Ouchi, A., Bard, E., Brannonot, P., Crucifix, M., Hewitt, C. D., Kageyama, M., Marti, O., Paul, A., Rosell-Melé, A., Waelbroeck, C., Weber, S. L., Weinelt, M., and Yu, Y.: A comparison of PMIP2 model simulations and the MARGO proxy reconstruction for tropical sea surface temperatures at Last Glacial Maximum, *Clim. Dynam.*, 32, 799–815, doi:10.1007/s00382-008-0509-0, 2009. 300, 301, 305

Peltier, W.: Ice age paleotopography, *Science*, 265, 195, doi:10.1126/science.265.5169.195, 1994. 299

20 Peltier, W.: Global glacial isostasy and the surface of the ice-age earth: the ICE-5G (VM2) model and GRACE, *Annu. Rev. Earth Pl. Sc.*, 32, 111–149, doi:10.1146/annurev.earth.32.082503.144359, 2004. 299, 302

Seidov, D., and Haupt, B. J.: Simulated ocean circulation and sediment transport in the North Atlantic during the Last Glacial Maximum and today, *Paleoceanography*, 12, 281, doi:10.1029/96PA03444, 1997. 299

30 Shin, S. I., Liu, Z., Otto-Bliesner, B., Brady, E. C., Kutzbach, J. E., and Harrison, S. P.: A simulation of the Last Glacial Maximum climate using the NCAR-CCSM, *Clim. Dynam.*, 20, 127–151, doi:10.1007/s00382-002-0260-x, 2003. 306, 309

Part 1: Experimental design and basic evaluation

M. Ballarotta et al.

Title Page

Abstract

Introduction

Conclusions

References

Tables

Figures



Back

Close

Full Screen / Esc

Printer-friendly Version

Interactive Discussion



- Spence, J.: Coarse versus eddy-permitting global ocean simulations: experiments with the UVic earth system climate model, Ph. D. thesis, University of Victoria, Canada, 2010. 300
- The FRAM Group: An eddy-resolving model of the Southern Ocean, *EOS T. Am. Geophys. Un.*, 72, 169, doi:10.1029/90EO00128, 1991. 300
- 5 Toggweiler, J. R., Russell, J. L., and Carson, S. R.: Midlatitude westerlies, atmospheric CO₂, and climate change during the ice ages, *Paleoceanography*, 21, PA2005, doi:10.1029/2005PA001154, 2006. 304
- Toracinta, E. R., Oglesby, R. J., and Bromwich, D. H.: Atmospheric Response to Modified CLIMAP Ocean Boundary Conditions during the Last Glacial Maximum, *J. Climate*, 17, 504–522, doi:10.1175/1520-0442(2004)017<0504:ARTMCO>2.0.CO;2, 2004. 299
- 10 Treguier, A. M., Theetten, S., Chassignet, E. P., Penduff, T., Smith, R., Talley, L., Beismann, J. O., and Böning, C.: The North Atlantic subpolar gyre in four high-resolution models, *J. Phys. Oceanogr.*, 35, 757–774, doi:10.1175/JPO2720.1, 2005. 300
- Weaver, A., Eby, M., Fanning, A. F., and Wiebe, E. C.: Simulated influence of carbon dioxide, orbital forcing and ice sheets on the climate of the Last Glacial Maximum, *Nature*, 394, 847–863, doi:10.1038/29695, 1998. 310
- 15 Yang, D., Myers, P. G., and Bush, A. B. G.: Sensitivity of the subpolar North Atlantic to Last Glacial Maximum surface forcing and sea ice distribution in an eddy-permitting regional ocean model, *Paleoceanography*, 21, 1–6, doi:10.1029/2005PA001209, 2006. 300

Part 1: Experimental design and basic evaluation

M. Ballarotta et al.

Title Page	
Abstract	Introduction
Conclusions	References
Tables	Figures
◀	▶
◀	▶
Back	Close
Full Screen / Esc	
Printer-friendly Version	
Interactive Discussion	

Table 1. Comparisons between the LGM- and PD-designed configurations, the model versions, atmospheric forcing variables and their frequency (d days, h hours and m months), bottom and surface conditions.

Experiments	LGM		PD
Model	NEMO-ORCA025	CCSM3	NEMO-ORCA025
Horizontal resolution	$\approx 0.25^\circ \times 0.25^\circ$	$\approx 1^\circ \times 1^\circ$	$\approx 0.25^\circ \times 0.25^\circ$
Vertical resolution	46 depth levels s	40 depth levels	46 depth levels
Atmospheric forcing	GFS1.0	COUPLED	DFS4.3
frequency u_{10}	6 h		6 h
frequency v_{10}	6 h		6 h
frequency rad_{sw}	1 d		1 d
frequency rad_{lw}	1 d		1 d
frequency t_2	6 h		6 h
frequency q_2	6 h		6 h
frequency precip	1 d		1 m
frequency snow	1 d		1 m
frequency runoff	1 d		1 m
Bathymetry	ICE-5G	ICE-5G	ETOPO2
Coupling Ocean/sea-ice	every 2 h	once a day	every 2 h

**Part 1: Experimental
design and basic
evaluation**

M. Ballarotta et al.

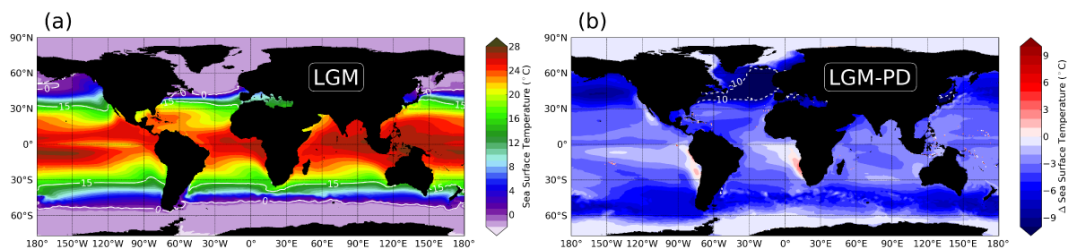


Fig. 1. Map of (a) the annually averaged Sea Surface Temperature (SST) in the LGM eddy-permitting simulation and (b) its difference (LGM-PD) from the PD simulation.

Title Page

Abstract

Introduction

Conclusions

References

Tables

Figures

◀

▶

◀

▶

Back

Close

Full Screen / Esc

Printer-friendly Version

Interactive Discussion



Part 1: Experimental design and basic evaluation

M. Ballarotta et al.

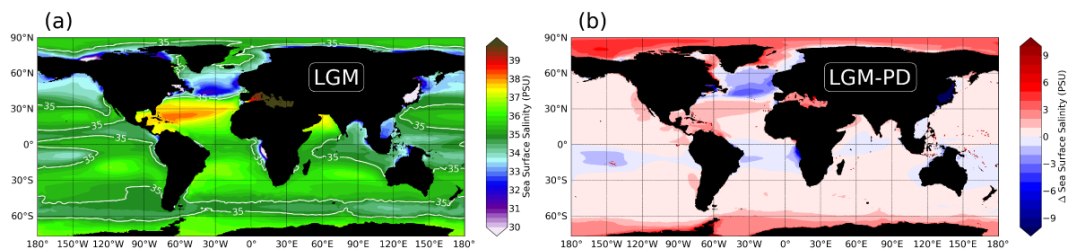


Fig. 2. Map of **(a)** the annually averaged Sea Surface Salinity (SSS) in the LGM eddy-permitting simulation and **(b)** its difference (LGM-PD) from the PD simulation.

Title Page

Abstract

Introduction

Conclusions

References

Tables

Figures

◀

▶

◀

▶

Back

Close

Full Screen / Esc

Printer-friendly Version

Interactive Discussion



Part 1: Experimental design and basic evaluation

M. Ballarotta et al.

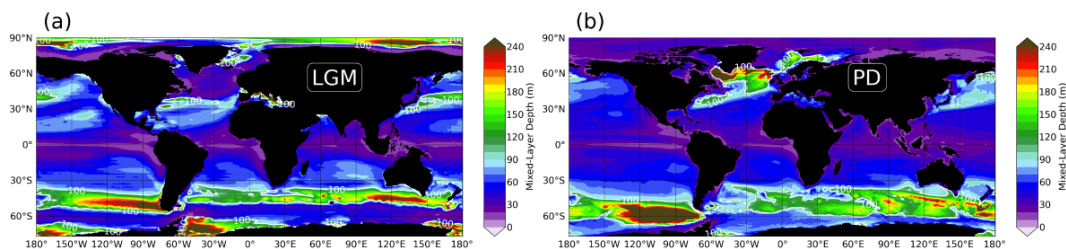


Fig. 3. Maps of the annually averages mixed-layers depth (MLD) in **(a)** the LGM and **(b)** the PD eddy-permitting simulations.

Title Page

Abstract

Introduction

Conclusions

References

Tables

Figures

◀

▶

◀

▶

Back

Close

Full Screen / Esc

Printer-friendly Version

Interactive Discussion



Part 1: Experimental design and basic evaluation

M. Ballarotta et al.

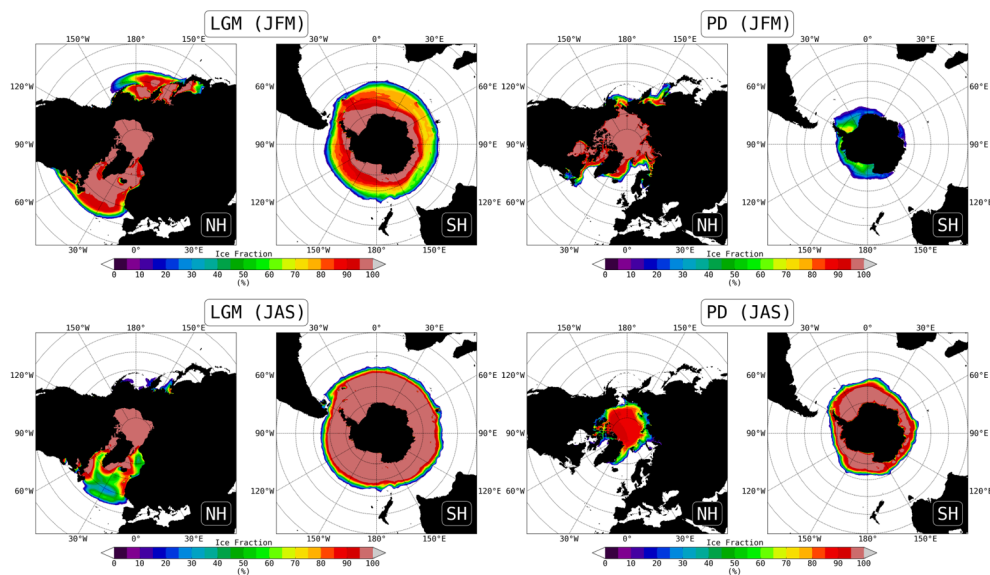


Fig. 4. Polar stereographic maps of the simulated sea-ice fraction (in %) for the boreal winter (JFM) and boreal summer (JAS) in the LGM and PD eddy-permitting simulations. Meridians are drawn every 30°, parallels every 10°.

Title Page

Abstract

Introduction

Conclusions

References

Tables

Figures

◀

▶

◀

▶

Back

Close

Full Screen / Esc

Printer-friendly Version

Interactive Discussion



Part 1: Experimental design and basic evaluation

M. Ballarotta et al.

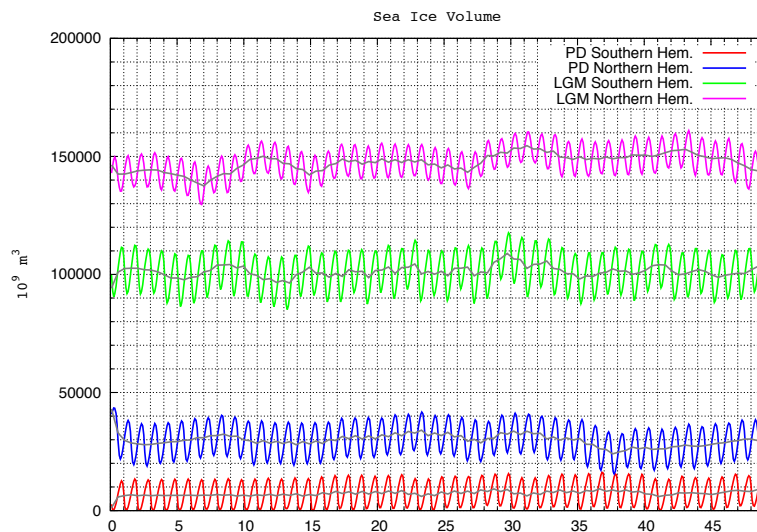


Fig. 5. Time series of the northern- and southern-hemispheric sea-ice volumes simulated in the PD and LGM experiments.

Title Page

Abstract

Introduction

Conclusions

References

Tables

Figures

◀

▶

◀

▶

Back

Close

Full Screen / Esc

Printer-friendly Version

Interactive Discussion



Part 1: Experimental design and basic evaluation

M. Ballarotta et al.

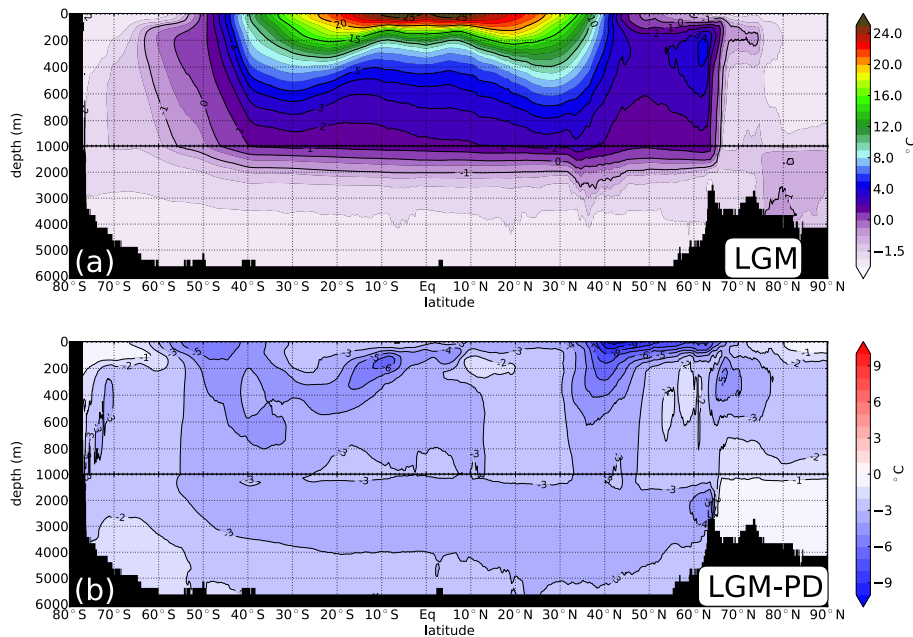


Fig. 6. Zonally- and annually-averaged temperature in (a) the LGM eddy-permitting simulation and (b) its difference (LGM-PD) from the PD simulation.

Title Page

Abstract

Introduction

Conclusions

References

Tables

Figures

◀

▶

◀

▶

Back

Close

Full Screen / Esc

Printer-friendly Version

Interactive Discussion

Part 1: Experimental design and basic evaluation

M. Ballarotta et al.

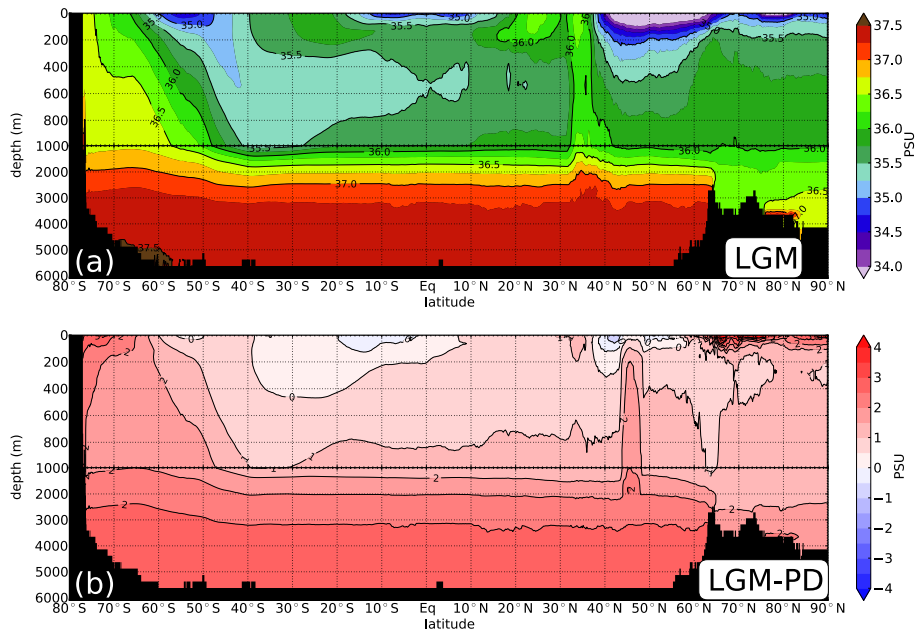


Fig. 7. Zonally- and annually-averaged salinity in (a) the LGM eddy-permitting simulation and (b) its difference (LGM-PD) from the PD simulation.

[Title Page](#)[Abstract](#)[Introduction](#)[Conclusions](#)[References](#)[Tables](#)[Figures](#)[◀](#)[▶](#)[◀](#)[▶](#)[Back](#)[Close](#)[Full Screen / Esc](#)[Printer-friendly Version](#)[Interactive Discussion](#)

Part 1: Experimental design and basic evaluation

M. Ballarotta et al.

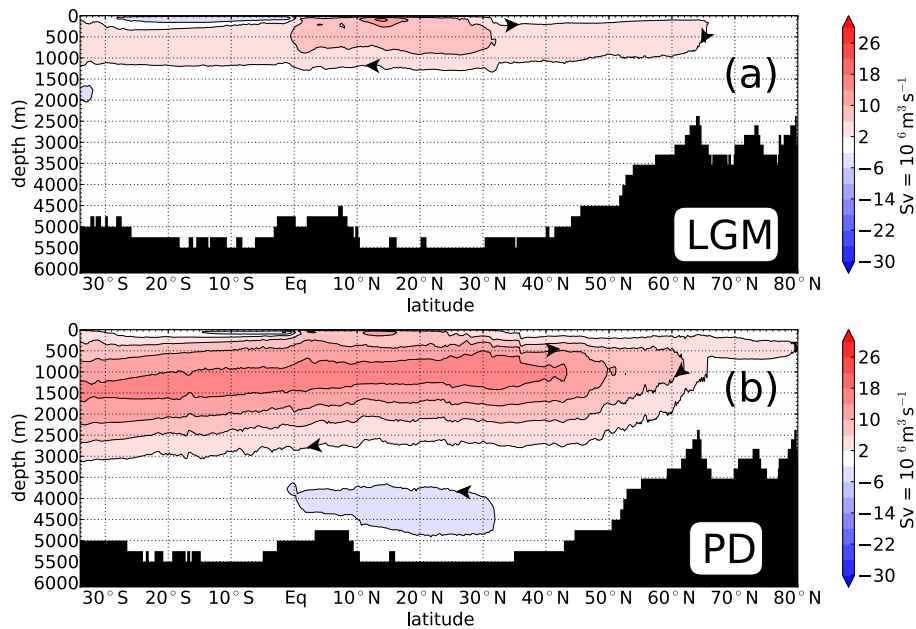


Fig. 8. Atlantic Meridional Overturning Stream function computed (a) for the LGM and (b) PD eddy-permitting simulations.

[Title Page](#)[Abstract](#)[Introduction](#)[Conclusions](#)[References](#)[Tables](#)[Figures](#)[◀](#)[▶](#)[◀](#)[▶](#)[Back](#)[Close](#)[Full Screen / Esc](#)[Printer-friendly Version](#)[Interactive Discussion](#)

Part 1: Experimental design and basic evaluation

M. Ballarotta et al.

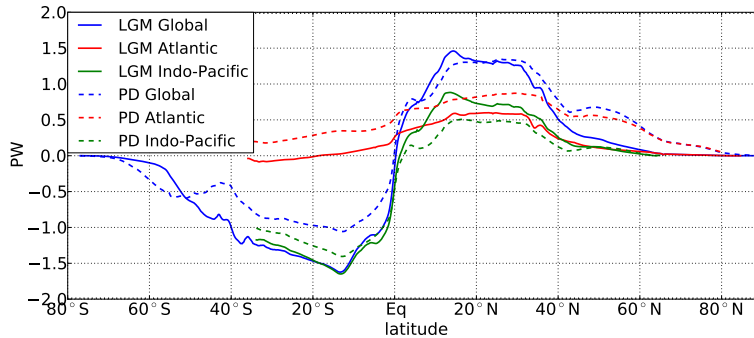


Fig. 9. Comparison of the meridional heat transport in PetaWatt (PW) computed for the LGM and the PD eddy-permitting simulations for the Global, Atlantic and Indo-Pacific basins.

Title Page

Abstract

Introduction

Conclusions

References

Tables

Figures



Back

Close

Full Screen / Esc

Printer-friendly Version

Interactive Discussion



Part 1: Experimental design and basic evaluation

M. Ballarotta et al.

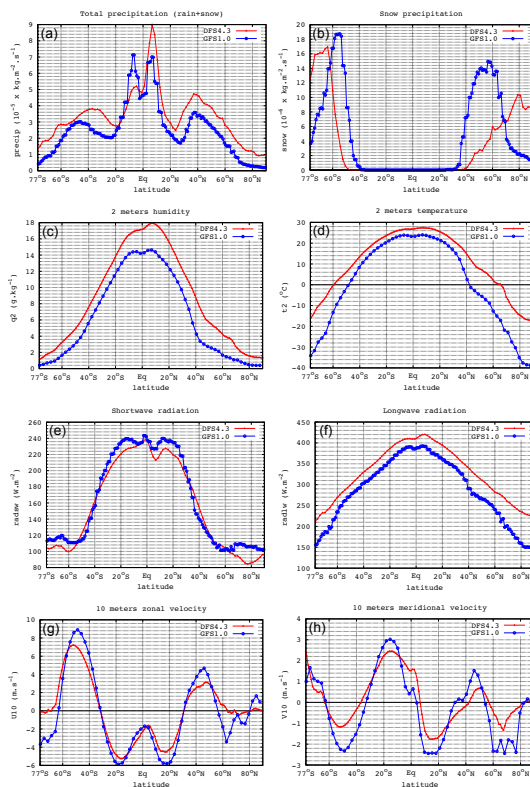


Fig. 10. Comparison of the zonally-averaged atmospheric surface fields (over the ocean) used to force the ocean model for the PD (DFS4.3), and the LGM (GFS1.0): **(a)** total precipitation, **(b)** Snow precipitation, **(c)** 2-m humidity, **(d)** 2-m temperature, **(e)** short-wave solar radiation, **(f)** long-wave radiation, **(g)** 10-m zonal velocity, **(h)** 10-m meridional velocity.

Title Page

Abstract

Introduction

Conclusions

References

Tables

Figures

◀

▶

◀

▶

Back

Close

Full Screen / Esc

Printer-friendly Version

Interactive Discussion